OPEN BIOLOGY

royalsocietypublishing.org/journal/rsob



Research

**Cite this article:** Steacy M, Didziokas M, Qiu T, Chathuranga DS, Liang C, Alazmani A, Moulding D, Gardner O, Moazen M, Pauws E. 2026 Mechanical bone loading effects on morphology and mechanobiology in the coronal suture of Crouzon mice. *Open Biol.* **16**: 250387.
https://doi.org/10.1098/rsob.250387

Received: 14 October 2025
Accepted: 27 February 2026

**Subject Areas:**
cellular biology, developmental biology

**Keywords:**
craniofacial system, biomechanics, mechanobiology, suture, craniosynostosis

**Author for correspondence:**
Miranda Steacy
e-mail: miranda.steacy.22@ucl.ac.uk

†These authors contributed equally to the study.

Electronic supplementary material is available online at https://doi.org/10.6084/m9.figshare.c.8382150.

THE ROYAL SOCIETY PUBLISHING

# Mechanical bone loading effects on morphology and mechanobiology in the coronal suture of Crouzon mice

Miranda Steacy[1,2,†], Marius Didziokas[1,†], Tengyang Qiu[1,2], Damith S. Chathuranga[1], Ce Liang[1], Ali Alazmani[3], Dale Moulding[2], Oliver Gardner[2], Mehran Moazen[1,†] and Erwin Pauws[2,†]

[1]Department of Mechanical Engineering, University College London, London, UK
[2]Department of Developmental Biology and Cancer, University College London Great Ormond Street Institute of Child Health, London, UK
[3]School of Mechanical Engineering, University of Leeds Faculty of Engineering and Physical Sciences, Leeds, UK

MS, 0009-0002-2296-9333; CL, 0000-0002-6789-1501; MM, 0000-0002-9951-2975

Craniosynostosis is a congenital condition characterized by the premature fusion of the craniofacial sutures. The Crouzon mouse ($Fgfr2c^{C342Y/+}$) is a well-established model of this condition which shows premature fusion of the coronal suture. Our group has recently shown that postnatal, cyclic loading can potentially rescue the coronal suture and normalize skull morphology in Crouzon mice. This study aimed to investigate the underlying biological mechanism of the treatment. Wild-type (WT) and Crouzon (MUT) mice underwent *in vivo* loading sessions. Loading did not significantly affect skull shape. The patency across the coronal suture did not change between treated and untreated MUT animals. Orientation and coherence of the coronal suture collagen fibres were statistically different when comparing WT untreated with MUT untreated and WT treated with MUT treated. Treatment increases the number of proliferative cells in both the WT and MUT sutures compared to their untreated counterparts. The mechanobiological mechanisms driving the differences need further investigation into molecular mechanotransduction pathways. Understanding the biological principles affected during bone loading, a more refined cyclical bone loading protocol can be developed and refined for potential clinical use.

## 1. Background

Craniosynostosis is a congenital condition characterized by the premature fusion of one or more sutures in the skull, occurring in approximately 1 in 2000 live births [1–3]. This early closure disrupts normal skull and brain growth, leading to complications such as abnormal head shape, vision and breathing difficulties, and developmental delays [4,5]. The impact of craniosynostosis can be profound for both patients and their families, in part due to the limited treatment options and the high risks associated with craniofacial surgical intervention. These treatments, which primarily involve invasive surgery, are most often tailored to each patient due to individual variation and the delicate nature of craniofacial surgery [6–8].

Several groups have recently explored alternative treatment approaches for craniosynostosis leveraging principles of tissue engineering and mechanobiology [9–12]. An example of these includes the application of external mechanical forces to the skull that have been shown to affect the overall skull morphology, suture structure and suture patency [13]. The field of dynamic bone loading is ever-growing, with promising results in animal models such

as rats, rabbits, pigs and mice [11,14–16]. Studies by Vij & Mao [16] and Moazen *et al*. [11] have demonstrated that external forces can delay suture fusion, with recent findings suggesting that dynamic loading of the frontal bone can prevent early fusion of the coronal suture and improve skull shape normalization in Crouzon mice ($Fgfr2c^{C342Y/+}$). However, despite extensive work on the morphological changes associated with mechanical calvarial bone loading, there has been little investigation into the mechanobiology underlying craniofacial remodelling.

External bone loading is believed to induce a mechanobiological response via a mechanotransduction pathway. Mechanotransduction refers to the molecular transformation of a physical stimulus to a biological response. An external mechanical stimulus can activate signalling pathways, up or downregulate gene expression and alter protein synthesis. On a cellular level, mechanotransduction can affect cell proliferation, migration, differentiation, angiogenesis and apoptosis [17–19]. On a tissue level, mechanotransduction can influence suture and bone architecture, shape and strength [18]. The extracellular matrix (ECM) is vital for transmitting mechanical loads and signals within the cell. The collagens and elastin transmit loads to the intracellular environment via integrins that connect the extracellular and intracellular structures, actin filaments and associated proteins that constitute the cytoskeleton [20]. While there is a large body of literature on endochondral mechanical loading and the mechanotransduction systems involved, research on the response of intramembranous and craniofacial bones to mechanical stimuli is limited [21,22]. This highlights an important gap in our understanding of mechanotransduction within the craniofacial system, as the pathway induced during cyclic bone loading has not been identified.

This study uses the Crouzon mouse model ($Fgfr2^{C342Y/+}$), developed in 2004 [23]. Crouzon syndrome is a gain-of-function mutation to the FGFR2 signalling pathway causing an increase in ligand-independent signalling [23,24]. The increase in FGF ligand binding affinity to the extracellular immunoglobulin-like domains causes constitutive activation of the pathway and allows binding without dimerization [25]. Mutations to the FGFR2 pathway are associated with a heterogeneous differentiative phenotype, suggesting an imbalance to the proliferative/differentiative switch [26]. Maintaining suture patency is not possible with FGFR2 mutations due to the disturbance to the delicate equilibrium of cell proliferation, differentiation, migration and apoptosis needed to regulate the osteogenic fronts at the cranial sutures [10]. In both humans and the mouse model, Crouzon syndrome presents primarily with early fusion of the coronal suture among other suture fusion, including the lambdoid suture and intersphenoid synchondrosis (ISS) [27]. Due to premature suture fusion, other phenotypic features, including midfacial hypoplasia, malocclusion and a domed-shaped skull, are observed [28–31]. The craniosynostosis phenotype typically begins to appear at embryonic stages (E18.5), with full fusion often occurring by postnatal day 20 (P20). In contrast, in the wild type the coronal suture remains patent [23,32].

The overall aim of this study was to further understand our previously observed improvements in skull morphology and investigate whether the suture patency was a result of mechanotransduction induced by cyclic bone loading. Specifically, we hypothesize that cyclic bone loading activates mechanotransduction in the coronal suture, which can be biologically observed by an increase in proliferative cells, promotion of angiogenesis through sprouting and enhancement of collagen fibre remodelling, ultimately leading to the observed improvements in skull morphology and suture patency.

# 2. Methods

## 2.1. Animals

$Fgfr2c^{C342Y/+}$ mice were maintained on a CD-1 genetic background [23]. The Crouzon mouse model (Fgfr2tm4Lni; aka $Fgfr2c^{C342Y}$; MGI:3053095) was re-derived at MRC Harwell (CD1-FGFR2c342y, number EM02488) through the European Mouse Mutant Archive (EMMA) at MRC Harwell.

In total, the study included 124 male and female animals, of which 75 were WT untreated, 10 were WT treated, 29 were MUT untreated and 10 were MUT treated. The number of treated animals remained consistent with Moazen *et al*. [11]. All the animals were used in morphological analyses with three from each group used for histological analyses. WT skulls used for histology were randomly selected, whereas selection for MUT skulls was based on suture patency observed in the CT data.

## 2.2. Mechanical loading

The cyclical loading treatment was adapted from Moazen *et al*. [11]. An experimental loading setup was developed with an actuator (T-LSR series, Zaber Technologies: res. 50 µm, max. load 200 N) and a force sensor (GSO Series, Transducer Techniques: res. 0.01 N with 1 N capacity) configured to a custom-developed LabVIEW program (National Instruments Corp, Austin, TX, USA). The treated mice underwent 10 loading sessions between the ages of P7 and P21. Loading sessions lasted 10 min at a frequency of 1 Hz and a force of 10 g (0.1 N). The loading tip was placed on the posterior aspect of the left frontal bone, lateral to the interfrontal suture and dorsally to the coronal suture. Post-mortem analysis was performed as described in figure 1.

## 2.3. Micro-CT analysis

The P21 skulls were immediately fixed in 10% formalin at 4°C for 7 days. The fixed skulls were scanned in a micro-CT scanner (XT H 225ST; Nikon, Herts, UK). CT images were imported into an image processing software (Avizo 2022.1; ThermoFisher Scientific, MA, USA) where the data were converted to 16 bit and the skulls were aligned using the image registration tool and reconstructed using a consistent threshold of 19 000 (figure 2A). Fifty-six landmarks were placed across the skull as shown

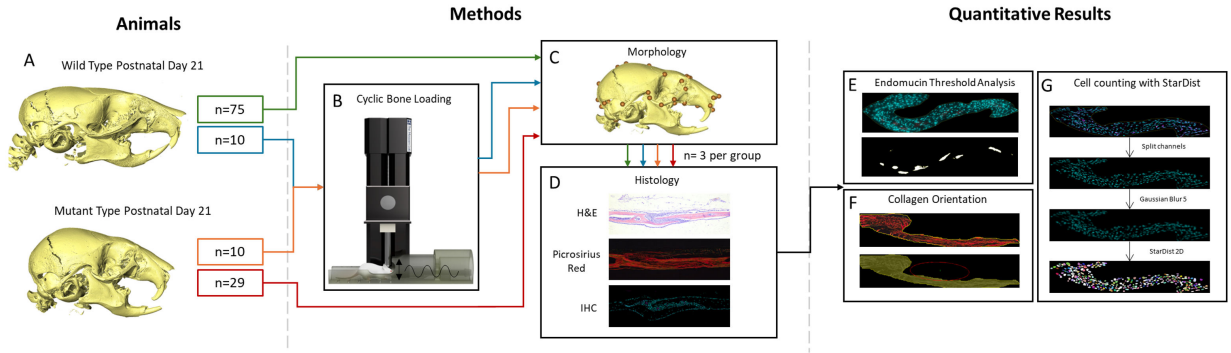


**Figure 1.** An overview of the experimental workflow performed**.** This includes the number of animals used for each experiment and the types of experiments conducted. (A) The number of WT and MUT animals in the loading treatment (blue and orange lines) and the control groups (green and red lines). (B) Cyclic bone loading experiment. (C) The morphological analysis undertaken. (D) The histology done including H&E, Picrosirius red and IHC. (E) The blood vessel analysis done in ImageJ via a threshold analysis. (F) The collagen fibre orientation analysis done in ImageJ with OrientationJ. (G) Cell counting in the coronal suture in ImageJ with StarDist.

in electronic supplementary material, figure S1. These were based on Richtsmeier *et al.* [33] and Motch Perrine *et al.* [34]. However, some changes were made to account for the fusion of various sutures in the Crouzon mice. Linear measurements were taken between landmarks 3 and 30 for length, 25 and 26 for width and 24 and 38 for height (electronic supplementary material, figure S1). PCA was carried out to evaluate the overall shape of the skulls (figure 2B). Finally, suture patency in the MUT coronal suture was investigated both qualitatively and quantitatively. Qualitatively, the MUT coronal suture was observed from the dorsal view of the skull where visible left and right coronal sutures were categorized as patent and no suture as fused (figure 2C). Partially patent MUT coronal sutures were categorized as patent, as only one control specimen out of all the investigated animals showed full patency highlighted in the quantitative analysis results. The qualitative analysis only observed the left and right coronal suture patency dorsally, thus even sutures with ventral fusion may be categorized as patent. Using the landmarks ([21–23]—see electronic supplementary material, figure S1, for landmark numbers), the coronal suture region was extracted from the rest of the skull and individual sagittal slices across the suture were categorized as fused or patent depending on whether there was a suture gaps in the slice (figure 2D) for quantitative patency. The landmarks were used to define the bounding box of the investigated region. The percentage of patent slices to the total number of slices was then recorded for each suture. The investigations were carried out for left and right coronal sutures individually. The advantages of the quantitative analysis were first, that the level of fusion could be quantified and second, that the entire depth of the suture is investigated to quantify true patency, rather than the dorsally apparent one. Micro-CT and histological analysis were done in parallel. The CT data validated the histology, confirming the overall shape of the suture, which could have changed during tissue processing. The histological slides and CT slices showed qualitative similarities in the suture morphology. Together, the two imaging techniques provided a holistic analysis of the overall shape of the coronal sutures and the changes throughout the skull.

## 2.4. Histological analysis

The fixed skulls were then washed in PBS and decalcified for 10 days in 20% EDTA at 4°C. The skulls were embedded in paraffin and sagittally sectioned 10 µm thick ($n$ = 3, each group). Sections were stained with haematoxylin and eosin and picrosirius red. Slides were imaged using the Zeiss Axioplan microscope. Picrosirius red was imaged with polarized light filters.

## 2.5. Immunohistochemistry

Sagittal sections were then placed in sodium citrate (10 mM tri-sodium citrate, 0.5% Tween-20, pH) and underwent antigen retrieval in a steamer. Primary antibodies were diluted with PBST (0.01% Tween-20), 10% donkey serum and 1% bovine serum albumin and applied overnight at 4°C. The following antibodies were used: PCNA (clone PC10(3F81), Invitrogen, 1 : 100), Cleaved Caspase3 (clone 9661S, Cell Signaling Technology, 1 : 300) and endomucin (clone V.7C7.1, abcam, 1 : 100). Secondary antibodies were applied with a 1 : 300 dilution. DAPI (4,6-diamidino-2-phylindole; Sigma) was pipetted and left for 10 min. Immunofluorescence imaging was done on the Zeiss Observer 7 at 20 × 1.6 NA, 20 × 1.0 NA and 10 × 1.0 NA objectives. Images were deconvolved using Huygens software and reconstructed in ImageJ.

## 2.6. Qualitative and quantitative analysis

The H&E images were compared to the CT scan to find the location of the H&E sections and validate the shape of the suture. Images were selected for qualitative analysis if they were void of artefacts (bone fragments, remaining wax, etc.), structurally sound (no obvious tissue tears or holes) and representative of all the imaged sutures. DAPI-stained images were used to do

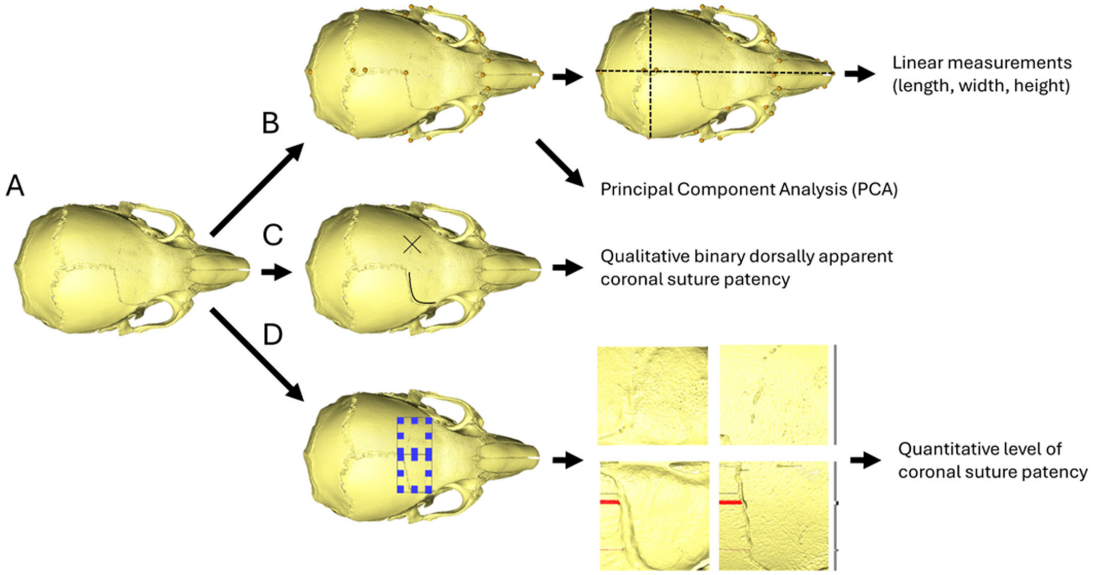


**Figure 2.** Overview of the CT analysis carried out. (A) Reconstructed and aligned MUT skull, (B) landmark placement, linear measurements and PCA, (C) binary qualitative dorsally apparent suture patency categorization and (D) qualitative level of suture patency analysis.

cell counting in ImageJ (v. 1.54i) ($n$ = 3 for each group, four technical replicates). An outline of the suture was manually drawn and the image was blurred (filter: gaussian, strength: 3). Cell counting was done by StarDist 2D (with CSBDeep) with a score threshold of 0.6 and an overlap threshold of 0.5 [35]. Proliferative cells were manually counted ($n$ = 3). Blood vessel area was found using a threshold analysis in ImageJ ($n$ = 3). Collagen orientation and coherence analysis was done using OrientationJ measure with the default settings (i.e. Laplacian of Gaussian (sigma) of zero) [36]. An outline of the suture was manually drawn and only the collagen fibres in the open suture area were included in the analysis. The 0° axis was aligned with the parietal bone. Images used for the analysis were selected from animals with full bilateral suture patency or left unilateral suture patency.

### 2.7. Statistical analysis

For linear measurement, morphometric analysis and quantitative suture patency analysis unpaired $t$-test with Welch's correction and Levene's test were performed. For apparent suture patency analysis, chi-squared test was used. For quantitative histological analyses, unpaired $t$-test with Welch's correction and Levene's test were performed. A $p$-value of <0.05 was considered significant.

## 3. Results

### 3.1. Morphometric analysis

Linear measurements taken across the landmarks (electronic supplementary material, figure S1) to quantify skull length, width and height did not highlight any statistically significant differences between the treated and untreated animals. Almost no differences were observed with the largest difference of a 1.61% (from 18.20 s.d. 0.71 mm to 18.49 s.d. 0.36 mm) increase of average skull length in the MUT treated animals ($p$ = 0.22) (figure 3A). Similarly, the shape analysis did not show statistically significant differences when comparing the principal components responsible for 95.00% of the variation observed (figure 3B). A statistically significant difference between WT and MUT animals was present for both treated and untreated animals in the principal component comparisons and all linear measurement comparisons except for the width measurements for the treated MUT versus. treated WT groups ($p$ = 0.21). There were no significant rescue effects on the skull shape and size at P21 immediately after the end of the loading procedure.

### 3.2. MUT coronal suture patency analysis

The qualitative analysis of the coronal suture patency highlighted an increase in the suture patency on the left (loaded) side of the skull from 27.59% of untreated MUTs with suture patency (8/29) to 60.00% of treated MUTs with suture patency (6/10). However, due to the lower number of animals in the loaded group, the result was not statistically significant at $p$ = 0.07. The increase on the right side was lower from 31.03% of untreated animals (9/29) to 40.00% of treated animals (4/10) ($p$ = 0.60) (figure 3C). Although, this analysis does not take into account the differences between bilateral and unilateral suture fusion. To account for this, each animal was recategorized by bilateral patency, unilateral patency and bilateral fusion (figure 3D). The treated and untreated MUT distribution of these categories was statistically significant ($p$ < 0.01). 7, 3 (1 left side, 2 right side) and 19 untreated MUT had bilateral patency, unilateral patency and bilateral fusion, respectively. In the treated MUT group 2, 6 (4 left

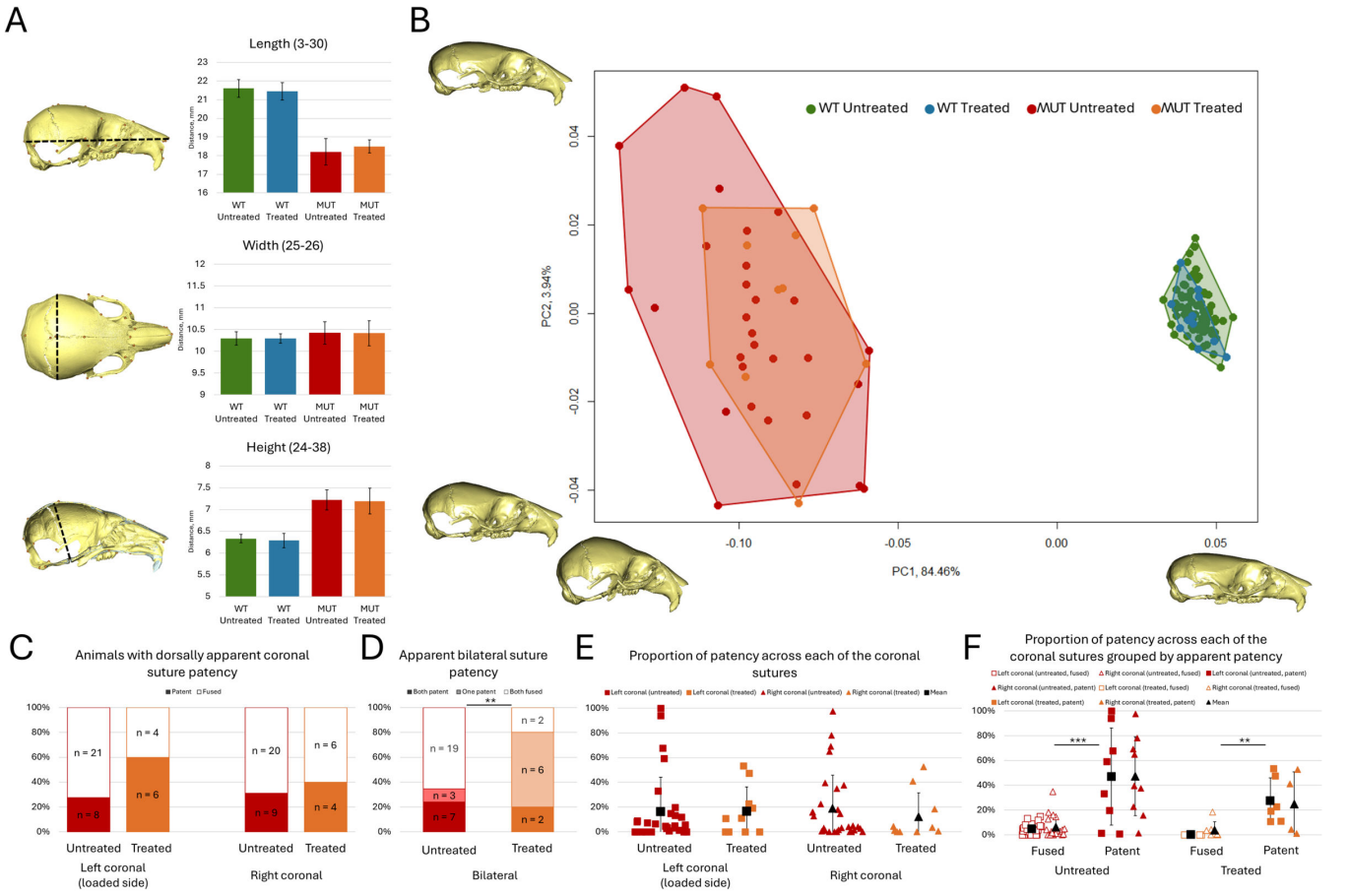


**Figure 3.** Overall skull morphology and suture patency results**.** (A) Linear measurements across the skull (length, width and height) numbers in the brackets indicate the measured landmarks. (B) PCA of shape comparing MUT treated and untreated and WT treated and untreated animals. (C) Qualitatively dorsally apparent suture patency in MUT animals (left and right sutures investigated individually). (D) Qualitatively dorsally apparent suture patency in MUT animals recategorized by bilateral patency, unilateral patency and bilateral fusion. (E) Quantitative comparison of suture patency in MUT animals. (F) Quantitative suture patency in MUT animals grouped by apparent qualitative suture patency.

side, 2 right side) and 2 had bilateral patency, unilateral patency and bilateral fusion, respectively. This highlights an increase in the incidence of unilateral coronal suture patency in the treated animals compared to the untreated animals. However, bilateral patency was marginally more common in the untreated group. The quantitative analysis did not show any increase in suture patency in either the left or right coronal suture (figure 3E). The quantitative suture patency was then grouped by apparent qualitative patency to investigate the possible connection between the quantitative and qualitative analysis. A statistically significant difference between the apparently patent suture and apparently fused sutures was observed in both untreated ($p < 0.001$) and treated ($p < 0.01$) animals in terms of quantitative suture patency percentage (figure 3F). Thus, if the sutures appeared patent qualitatively, they were more patent on average than the ones that did not appear patent. It should be noted that some of the apparently patent sutures did not show any quantitative patency.

## 3.3. Qualitative analysis of the coronal suture in P21 WT and MUT mice

CT data and histological analysis were done in parallel, which showed qualitative similarities in suture morphology (figure 4). Sutures are primarily composed of mesenchymal stem cells (MSCs) and collagen fibres making them important sites of bone growth and mechanical flexibility [4]. Both H&E and picrosirius red staining were performed to investigate the coronal suture cell and fibre organization, respectively, in all groups. In the WT mouse, the patent coronal suture separated the overlapping frontal and parietal bones with a dense population of MSCs and collagen fibres (figure 5A–C). The frontal bone thinned and hooked down, making up the inferior border, whereas the parietal bone tapered up, creating the superior border. The bones remained parallel, and the overall suture complex maintained a uniform width. The mechanically loaded WT mouse coronal sutures were visually indistinguishable from their control counterparts, possessing the same overall shape and geometry (figure 4A–F).

At P21 in the MUT mouse, the coronal suture could be either fused or patent (figure 5D–H). The fully fused MUT sutures lacked a distinguishable frontal–parietal division, MSCs and collagen fibres (figure 5G,H). The fused suture site presented with collagen-free nuclei-filled cavities. The presence, size and shape of the cell-filled cavities varied between individuals. Fully fused sutures were often thicker than the frontal and parietal bones. The MUT fused sutures were enlarged inferiorly increasing the thickness/height (electronic supplementary material, figure S2).

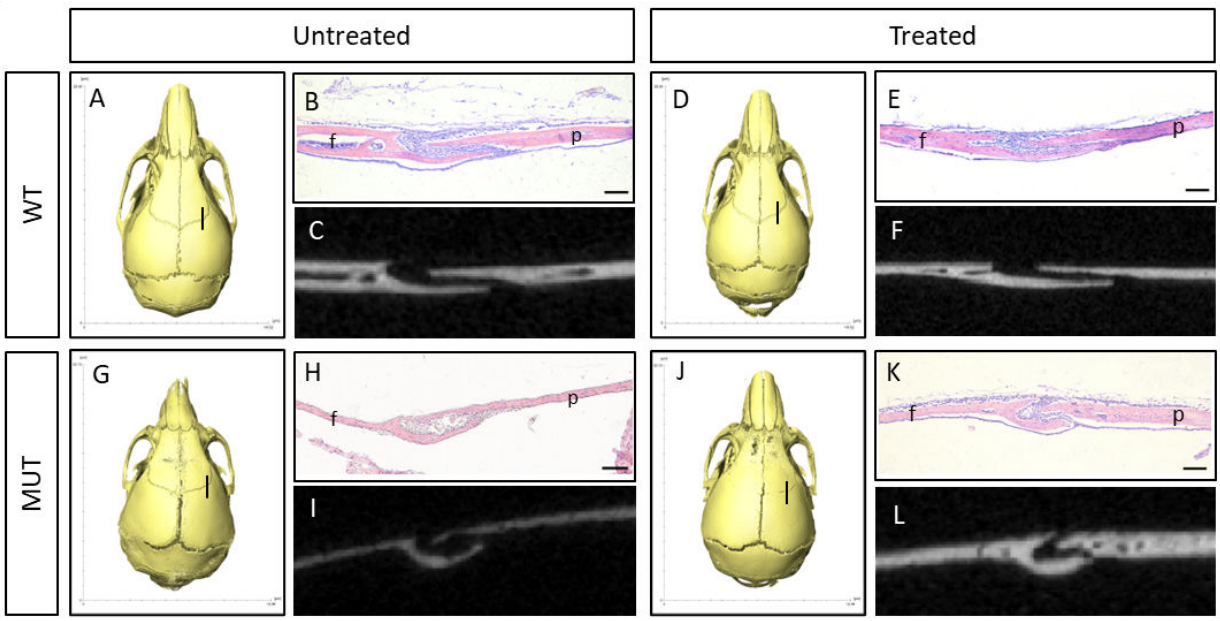


**Figure 4.** CT and histological imaging of the coronal suture in untreated and treated WT and MUT mice**.** (A,D,G,J) Coronal view of CT-scan skull reconstructions with landmarks denoting the position of the H&E-stained sections. (B,E,H,K) H&E sagittal section of the coronal suture. (C,F,I,L) CT-scan Ortho slice of the corresponding H&E section. The reconstructed CT scans and histology selected for this figure are representative of slices observed in each category where sutures are patent. f, frontal; p, parietal. Scale bar: 100 µm.

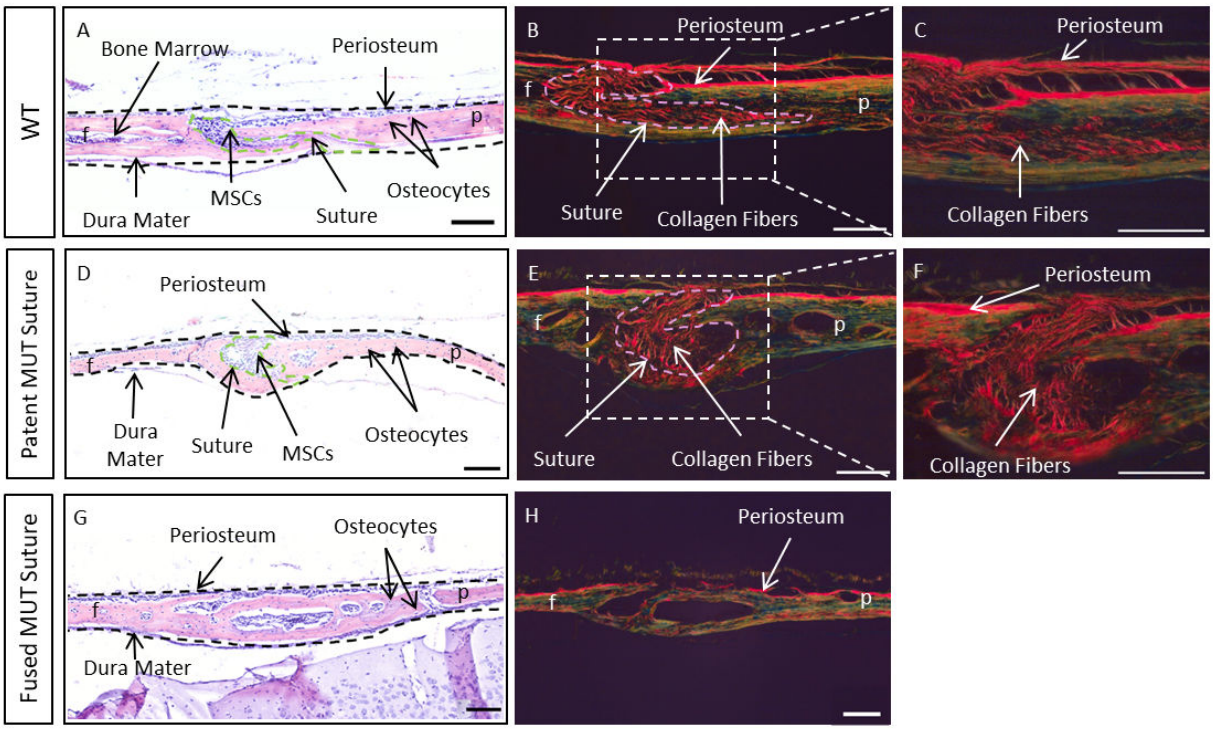


**Figure 5.** Comparative histology of the coronal suture in untreated WT, untreated patent MUT and untreated fully fused MUT mice. (A) H&E-stained sagittal section of a WT coronal suture with labels identifying the different elements of the coronal suture complex. The coronal suture remains patent in the WT. (B,C) Picrosirius red -stained sagittal section of a WT coronal suture imaged under a polarized filter. The suture remains open, filled with collagen fibres (D) H&E-stained sagittal section of a MUT patent coronal suture. The coronal suture in the MUT mouse has remained patent. (E,F) Collagen fibres are still present in the MUT patent suture. (G) Fully fused coronal suture in a MUT, no presence of a suture complex. (H) Absence of collagen fibres in the cavities. MSCs, mesenchymal stem cells; f, frontal; p, parietal. Scale bar: 100 µm.

When the MUT coronal suture remained patent, it was possible to identify the frontal and parietal bones (figure 4D–F). The downward hook of the frontal bone was often conserved, whereas the morphology of the parietal bone varied not only between animals but between histological sections of the same suture. The area between the two bones was filled with MSCs and collagen fibres, occupying any available space. The patent MUT suture presented with a prominent inferior bulge which give the suture an overall oval shape.

Comparing WT, patent MUT and fused MUT highlighted that WT and patent MUT sutures had MSCs and collagen fibres, and fused MUT sutures did not. The patent MUT sutures still maintained a suture joint, whereas the fused MUT sutures had

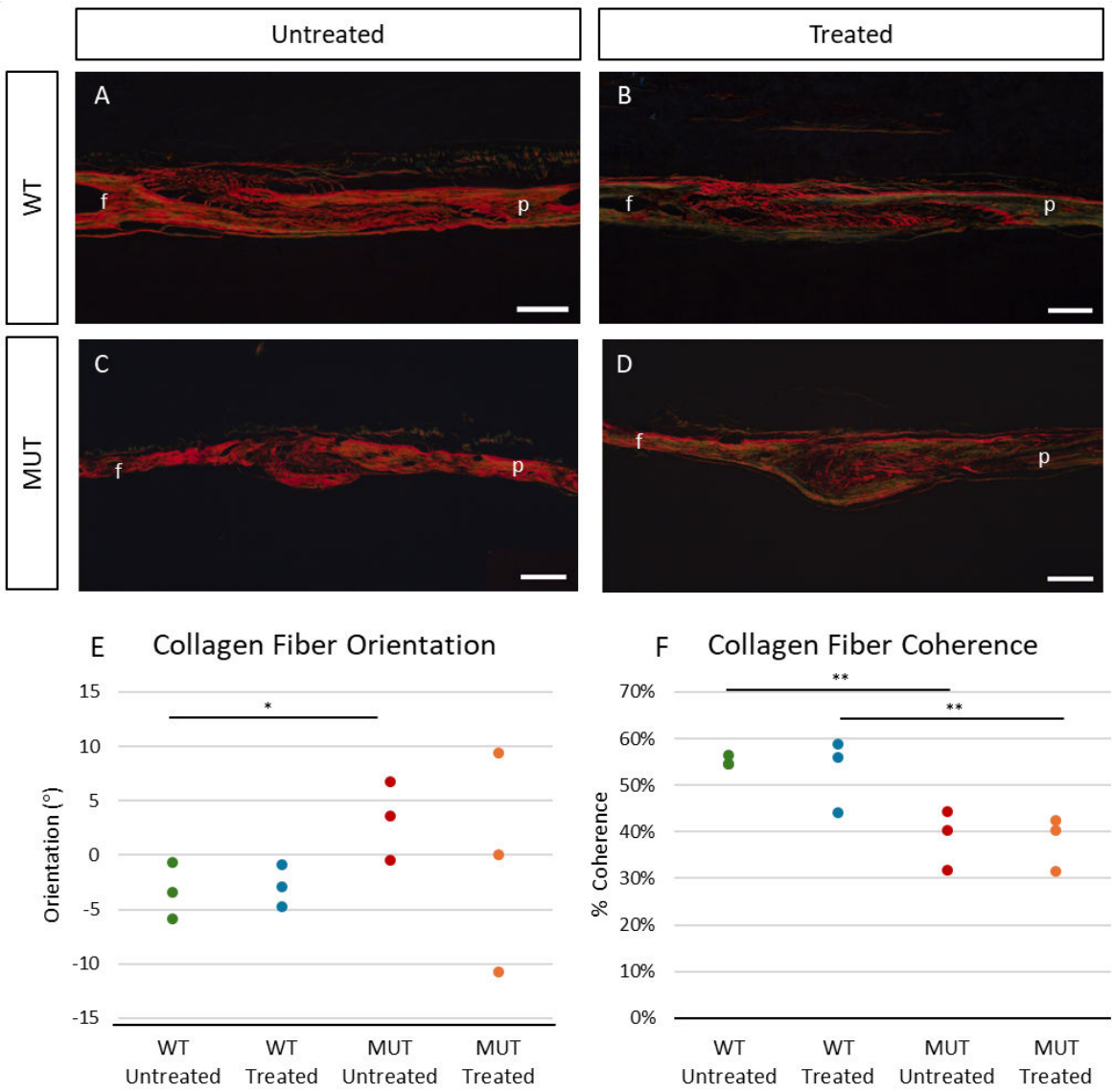


**Figure 6.** Picrosirius red-stained sagittal sections of coronal sutures and quantitative analysis**.** (A) WT untreated, (B) WT treated, (C) MUT untreated, (D) MUT treated. f, frontal; p, parietal. Scale bar: 100 µm. (E) Collagen fibre orientation. Orientation had a statistically significant *t*-test between WT untreated and MUT untreated ($p < 0.045$). (F) Collagen fibre coherence. Coherence has a statistically significant *t*-test when comparing WT untreated with MUT untreated ($p < 1.54E{-}06$) and MUT treated ($p < 1.02E{-}08$) and WT treated with MUT treated ($p < 6.9E{-}06$) ($n = 3$, four technical replicates per group). *$p < 0.05$; **$p < 0.01$.

complete loss of a fibrous suture joint. MUT sutures, regardless of patency, were inferiorly enlarged and showed more intra- and inter-morphological variation than the WT coronal sutures.

## 3.4. Quantitative collagen analysis

Collagen fibre orientation is important for normal cellular activity and promoting new bone growth. Orientation and self-assembly of the ECM can be influenced by external mechanical stimuli, meaning that rescuing collagen fibre orientation to a WT phenotype in the MUT suture may be a consequence of the mechanical bone loading [37–39]. Collagen fibres in the coronal sutures were analysed using OrientationJ Measurement in ImageJ (Fiji). This tool calculated the directional coherency coefficient of the fibres, generated an overall degree of orientation and a coherence number. A coherency coefficient of 100% indicates a fully uniform orientation of the fibres (figure 6). The 0° axis was aligned with the parietal bone and only the collagen fibres in the coronal sutures were analysed.

Orientation relative to the dorsal surface of the frontal bone was significantly different when comparing WT untreated with MUT untreated ($p < 0.05$). The collagen orientation in MUT untreated (3.27° s.d. 6.33°) and treated (−0.44° s.d. 11.26°) had larger standard deviations when compared to their WT untreated (−3.34° s.d. 3.09°) and treated (−2.83° s.d. 2.35°) counterparts. There was no statistically significant difference between WT untreated and WT treated, WT treated and MUT treated or MUT untreated and MUT treated. The MUT sutures had large inter-variance of collagen fibres, meaning each MUT animal had a unique, disorganized collagen matrix. Comparatively, the WT sutures had lower standard deviation values, reflecting a more uniform orientation between samples. With average values of −3.34° and −2.83° and low standard deviations, relative to MUT sutures, WT collagen fibres were more often closely aligned with the parietal bone (0° axis) compared to their MUT

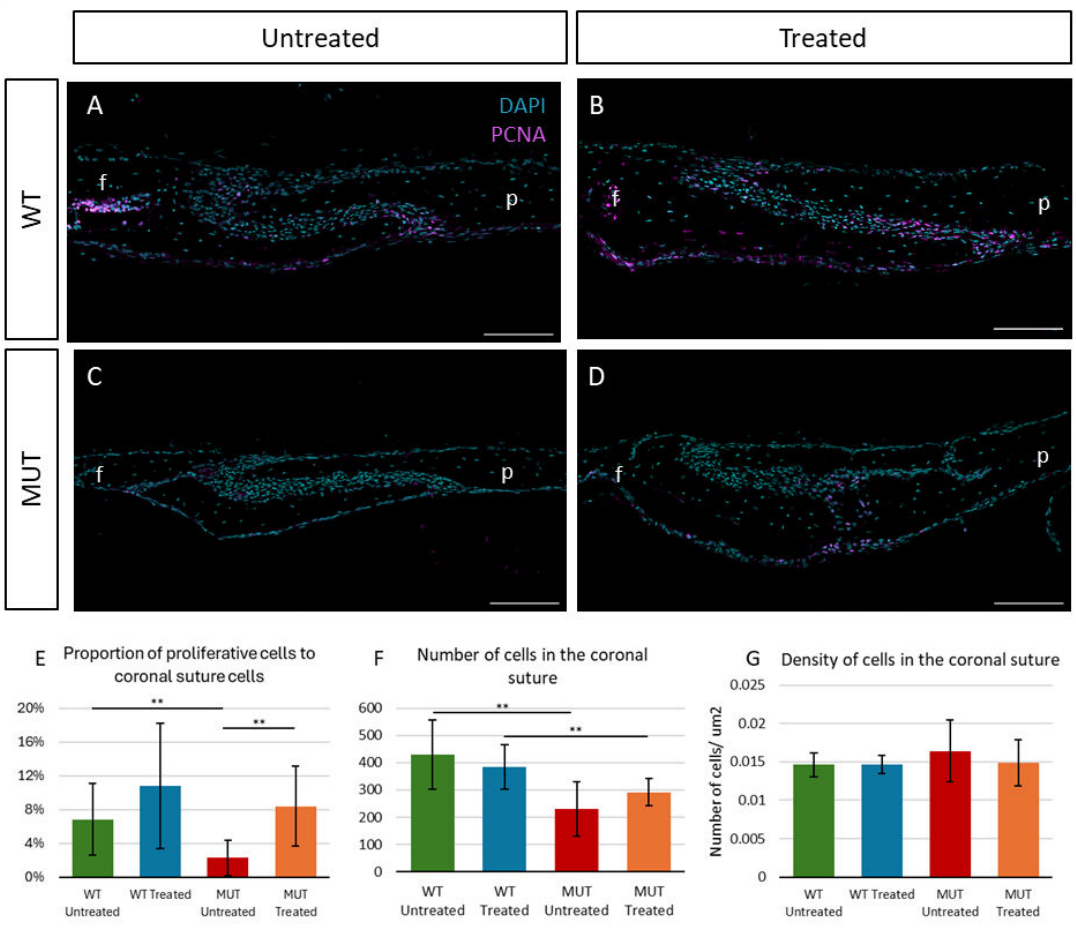


**Figure 7.** Immunofluorescence-stained for PCNA (magenta) and DAPI (blue) sagittal sections of coronal suture and quantitative analysis. (A) WT untreated, (B) WT treated, (C) MUT untreated and (D) MUT treated. f, frontal; p, parietal. Scale bar: 100 µm. (E) Proportion of proliferative cells to coronal suture cells. (F) Number of cells in the coronal suture. (G) Density of cells, number of cells per micrometre ($n = 3$, four technical replicates per group). $^{**}p < 0.01$.

counterparts. Overall, this analysis showed that MUT sutures have abnormal collagen fibre orientation and mechanical loading did not have any significant effect in altering their collagen fibre orientation.

There was no statistically significant difference in coherence between WT untreated and WT treated ($p = 0.35$) or between MUT untreated and MUT treated ($p = 0.78$). MUT untreated had an average coherence value of 38.83% s.d. 7.61% and MUT treated had an average of 38.09% s.d. 5.15%. WT untreated and treated coherences were 55.20% s.d. 4.25% and 52.93% s.d. 7.11%, respectively. There was a statistically significant difference in coherence when comparing WT untreated with MUT untreated ($p < 0.001$) and WT treated with MUT treated ($p < 0.001$). The higher coherence percentages, seen in the WT, illustrated the general uniformity of the collagen fibre orientation in the coronal suture. This contrasted with the lower coherence percentages seen in the MUT, indicating a more disorganized collagen matrix in the coronal sutures. The treatment in neither of the WT and MUT groups affected the organization of the collagen fibres in the coronal suture.

## 3.5. Proliferation assay

The proportion of proliferative cells in the coronal suture was calculated by manually outlining the coronal suture, counting the number of DAPI-stained cells using StarDist and manually counting the amount of proliferative cells [35] (figure 7). The WT-treated group had the largest proportion of proliferative cells with an average of 10.78% s.d. 7.41% of cells being proliferative (figure 7E). The MUT treatment group had the second highest proportion of proliferative cell with an average of 8.39% s.d. 4.75%. The WT untreated group had an average of 6.84% s.d. 4.21% and the MUT untreated had the lowest number of proliferative cells with an average of 2.27% s.d. 2.11%. The WT and MUT untreated groups had a statistically significant difference in proliferation ($p < 0.005$), meaning that MUT mice had lower baseline levels of proliferation in the coronal suture than their WT counterparts. Additionally, the MUT treated and untreated groups were significantly different ($p < 0.001$). These findings indicate that the treatment increased the number of proliferative cells in the MUT suture compared to its untreated counterparts. The WT-treated and MUT-treated proliferation levels were not statistically significant. Instead, the MUT treated (8.39% s.d. 4.75%) proliferation proportion was most similar to that of the untreated WT (6.84% s.d. 4.21%), illustrating that the treated MUT suture resembles a more normal suture. This finding may indicate that loading may allow the MUT suture to be rescued to an untreated baseline level of WT proliferation.

The next test examined whether differences in mitotic proportion impact the overall cell number in the suture. The number of cells in the coronal suture was the highest in the WT untreated sutures with an average of 429.83 s.d. 127.63 cells (figure 7F). WT treated mice had an average of 383.25 s.d. 81.40 cells. MUT untreated and treated had 230.67 s.d. 98.69 cells and 291.42 s.d.

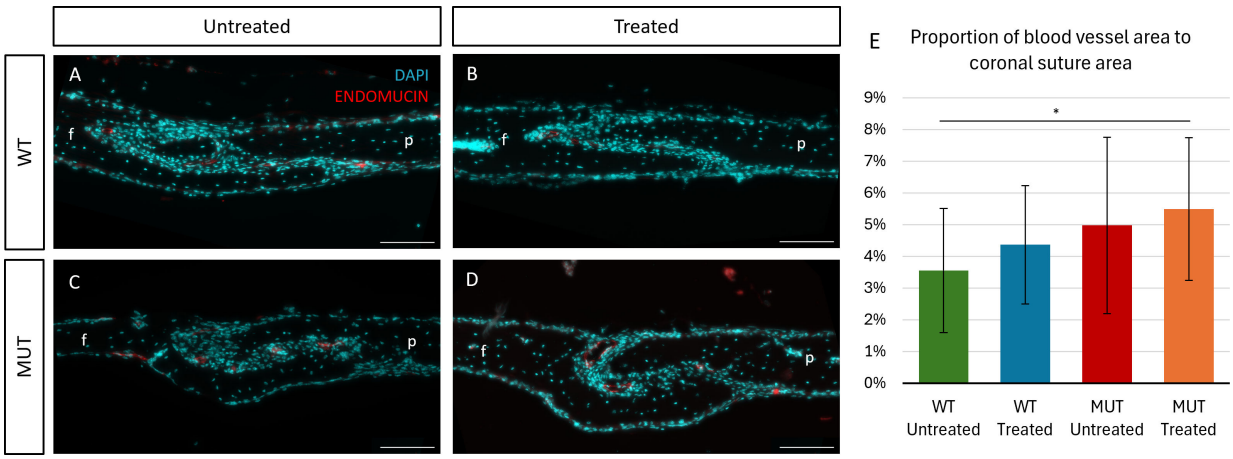


**Figure 8.** Immunofluorescence-stained for endomucin (red) and DAPI (blue) sagittal sections of coronal suture. (A) WT untreated, (B) WT treated, (C) MUT untreated and (D) MUT treated. f, frontal; p, parietal. Scale bar: 100 µm. (E) Proportion of blood vessel area to coronal suture area. The blood vessel area analysed included solely the endomucin-stained area and did not include the lumen ($n = 3$, four technical replicates per group). *$p < 0.05$.

49.51 cells on average, respectively. WT untreated and treated coronal sutures did not have a statistically significant difference in the number of cells ($p = 0.30$) and neither did MUT untreated and treated sutures ($p = 0.07$). WT and MUT untreated mice had statistically significant differences in the number of cells in the coronal suture ($p < 0.001$) as well as WT and MUT treated ($p < 0.005$). Following the counting of suture cells, the density of the cells in the coronal suture was calculated. The average density in the WT untreated and treated was the same, both with 0.0146 cell µm$^{-2}$, MUT untreated was 0.0164 cell µm$^{-2}$ and MUT treated was 0.0148 cell µm$^{-2}$ (figure 7G). None of these averages were statistically significant meaning that regardless of genotype or treatment cell density in the coronal suture remained consistent. However, combined with the proliferation data, this trend towards an increased number of cells—closer to that of WT sutures—in treated MUT sutures compared to untreated MUT sutures, may support a more patent suture.

### 3.6. Blood vessel analysis

Blood vessels in the coronal suture were observed using an endomucin antibody. Endomucin is found in the capillary endothelial cells. The proportion of blood vessel area to coronal suture area was calculated by a threshold analysis in ImageJ (figure 8). The WT untreated group had an average of 3.56% s.d. 1.95% of the coronal suture area occupied by blood vessels. The WT treated had an average of 4.37% s.d. 1.87%, MUT untreated had a 4.98% s.d. 2.78% average and MUT treated averaged at 5.49% s.d. 2.25%. The following groups were not statistically significant: the WT untreated and treated ($p = 0.31$), MUT untreated and treated ($p = 0.63$), WT and MUT untreated ($p = 0.16$) and WT and MUT treated ($p = 0.20$). None of the groups was statistically significantly different from one another except for the WT untreated and MUT treated ($p < 0.05$). Although not statistically significant, the treated groups showed an increase in blood vessel area compared to their untreated counterparts and MUT coronal sutures had a greater blood vessel area than WT.

## 4. Discussion

A previous study by Moazen *et al*. [11] found that cyclic bone loading delayed the early fusion of the coronal suture in the Crouzon mouse (MUT). This study aimed to further understand the associated improvements in skull morphology and whether the suture patency improvement was due to a mechanobiological effect induced by cyclical bone loading. The main finding from this study is that cyclical bone loading induces proliferation in the suture. Furthermore, cyclical loading showed no effect on the orientation of the collagen fibres in the coronal sutures after loading.

Morphological analysis investigated the gross shape differences between the treated and untreated animals in both WT and MUT animals. No statistically significant differences were observed between the treated and untreated groups across linear measurements and overall skull shape. However, the skull shape of the WT animals was statistically significantly different to the skull shape of the MUT animals in both treated and untreated groups. Similar differences were observed in the linear measurements with a single exception of width between WT and MUT treated animals.

The present study failed to replicate the statistically significant increase in skull length observed in Moazen *et al*. [11]. The original scans from the previous study were reconstructed and landmarked following the same landmarking scheme. The lack of treatment effect in the current study was not due to the landmark scheme (electronic supplementary material, figure S3). The comparison of the linear measurements between the two studies highlights differences between the phenotypes in the control animals. Additionally, while four of the 31 MUT animals (both treated and untreated) included in the Moazen *et al*. [11] study had patent ISS in the skull base, none of the 39 MUT included presented with patent ISS. These differences highlight significant phenotypic differences between the MUT populations of the two studies (specifically, more severe phenotype in the current study) which may in turn explain the lack of phenotypic rescue observed in this study.

The lack of treatment effects on the skull shape, in the current study, may be linked to the observed lack of an effect on quantitative suture patency. The apparent suture patency as observed from the dorsal view of the skull did increase on the left (loaded) side (not statistically significant) and the incidence of unilateral apparent patency increased significantly in the treated MUT group compared to their untreated counterparts. More animals proportionally had bilateral apparent patency in the untreated group. The treatment did not show any effect on the quantitative coronal suture patency. The qualitative suture analysis only took into account the most dorsal part of the suture to gauge fusion, where the quantitative analysis considered the full depth of the suture. The discrepancy in the results here may highlight that the loading had an effect on the dorsal part of the coronal suture, but not on the more ventral parts where fusion tends to originate. While the quantitative suture patency methodology introduced here likely captures the physical patency better, the comparison to qualitative suture patency analysis was maintained to retain comparability with the analysis performed by Moazen *et al*. [11].

Importantly, the sutures play a mechanical role in permitting skull growth during brain expansion and external loading [40–42]. However, with the treatment effects limited to the dorsal part of the suture, the dorsal patency may not sufficiently permit deformation across the full suture as seen in the WT animals. This could explain the lack of therapeutic effects on the skull shape observed in this work. Additionally, it is unclear how much the premature fusion of the coronal suture affects the craniofacial shape in this mouse model. The premature fusion of the coronal suture has been considered one of the main drivers of the phenotype. However, with quantitative investigation of the level of coronal suture patency the correlation between the linear measurements and shape against the level of patency can be investigated in untreated MUT animals (electronic supplementary material, figure S4). One potential reason for minimal therapeutic effects on suture patency and, thus, the overall morphology may be attributed to the fusion of the coronal sutures before the beginning of the loading treatment. As shown by Didziokas *et al*. [43], not only are the sutures fused at P7 but also the fusion significantly restricts suture deformation with no statistically significant increase in suture width during loading. The patent sutures in the WT animals, as shown in the previous study, permit deformation ranging from 0.33 times the original length to 4.37 times. This restriction of mechanical strain across the loaded MUT suture may contribute to the lack of clear suture phenotype rescue. In short, the coronal suture patency did not correlate strongly with any of the linear measurement or PC1 that largely captured the differences between MT and WT skull shapes. This is contrary to other mouse models of craniosynostosis such as Twist1,$^{+/-}$ where natural bilateral coronal suture patency did lead to a more WT-like skull shape even at P15 [44]. Thus, suggesting that even full patency rescue of the coronal suture is unlikely to significantly rescue the craniofacial shape in the Crouzon mice, perhaps due to the synchondrosis fusion in the skull base [28].

The qualitative observation of the histology showed that mechanical bone loading in the WT coronal sutures did not cause adverse effects when compared to the untreated WT coronal sutures. In the MUT coronal suture, there was a clear qualitative difference between locally open and fully fused sutures in both treated and untreated groups. The patent MUT sutures had a distinguishable frontal–parietal delineation, MSCs and collagen fibres. The fully fused MUT coronal sutures did not have a delineation between the frontal and parietal bones. Instead, the fully fused suture area was enlarged and had nuclei-filled cavities void of collagen fibres. The absence of collagen fibres in the nuclei-filled cavities indicated that, with suture fusion, there was a complete loss of the fibrous tissue, and the cavities did not have the same characteristics as a suture. Instead, the cavities resemble bone marrow niches, but without cellular labelling, the function or identity of these cavities remains unknown. Although Zimmermann *et al*. [45] described a key step of suture development at P20 that involves the enlargement of bone marrow cavities. This reinforces the hypothesis that the fully fused MUT sutures are perhaps filled with bone marrow cavities instead of a fibrous suture. The absence of collagen fibres in the fully fused coronal suture suggests that once full fusion occurs the mechanisms of suture recovery are likely different from the patent suture retention mechanisms.

Proliferation in the WT untreated coronal suture was higher than in the MUT untreated. Eswarakumar *et al*. [23] observed a similar proliferation patterns, finding that the Fgfr2c$^{C342Y/+}$ had increased proliferation in the coronal suture cells during the early stages of development and saw a decline after birth. This suggests that the increased number of proliferative osteoblast cells in the coronal suture at E14.5, but not later may lead to the premature fusion of the frontal and parietal bones seen postnatally [23]. Additionally, Iseki *et al*. [46] propose that an increase in fibroblast growth factor signalling downregulates *Fgfr2* and inhibits cell proliferation in the coronal suture. The treatment in the MUT mice showed a statistically significant increase in the proportion of proliferative cells. A non-statistically significant increase was observed in the WT-treated mice compared to their untreated counterpart. These findings may suggest that the loading treatment regardless of the phenotype does induce proliferation. This increase in proliferation may be due to the primary cilia stimulation. Primary cilia modulate osteogenic mechanotransduction pathways, particularly in the MSCs [47]. Stimulating the primary cilia enhances the expression of osteogenic genes including COX-2 and BMP2 in MSCs, increasing the proliferation rate in MSCs twofold [48]. The observed increase in proliferation may also be due to paracrine communication specifically via the expression of PGE2. The expression of PGE2 via mechanical stimulation has been shown to increase preosteoblast proliferation [49]. Further investigation is needed into the pathways involved in the observed proliferation increase. In addition to a proliferation marker, an apoptotic assay was undertaken. The coronal suture tissue did not present with notable apoptotic markers in any of the investigated groups (electronic supplementary material, figure S5).

Although proliferation was increased in the treated animals, there were no significant differences in cell density of the patent coronal sutures between groups. The density of cells remained consistent between groups, but the number of cells in the coronal suture varied between groups. WT sutures had a higher number of cells in the coronal suture compared to the MUT sutures. This highlights that the WT sutures are larger in area but not more densely packed.

The collagen fibres in the suture provide strength and flexibility to the skull and allow for normal cellular activity including migration, proliferation and differentiation [20]. Oriented collagen fibres scaffolds can promote new bone growth and induce cells to secrete ECM with orientation structure [38]. In *in vitro* systems, fluid shear stress and shear stress have been shown

to influence collagen fibre orientation and self-assembly [37–39]. The ECM is made of a network of macromolecules including glycosaminoglycans (GAG), proteoglycans, collagens, fibronectin and other glycoproteins [50]. The suture ECM is made of Sharpey's fibres, consisting mainly of type 1 collagen fibres [51]. The composition and structure of the ECM are important for cellular adhesion, migration, proliferation and differentiation [52]. In Crouzon's syndrome, GAG, sulfated GAG and fibronectin accumulation are reduced and collagen secretion is increased [50]. Sulfated GAG is responsible for collagen fibre orientation and affects matrix mineralization [53]. The drop in sulfated GAG alters collagen fibril orientation, impairing bone remodelling. The abnormal ECM expression pattern in Crouzon syndrome damages the formation and maintenance of the connective tissue architecture [50].

When the ECM is exposed to mechanical stimuli, it undergoes remodelling and changes its internal microstructure [20]. ECM remodelling is important for maintaining tissue homeostasis, activating integrin signalling pathways like RhoA/ROCK to drive cellular mechanotransduction and stimulating MSC differentiation [54, 55]. The ECM in the coronal suture was observed to see if cyclic bone loading allowed collagen fibre remodelling to a more wild-type phenotype in an effort to promote suture patency. The coronal suture in the WT mice showed a higher coherence values, meaning more organized matrixes. Quantitative analysis of collagen fibres showed significant differences in the coherence between WT untreated and MUT untreated, as well as between WT treated and MUT treated. The smaller coherence results in the MUT coronal sutures highlight the general disorganized collagen matrix. No recovery of the collagen fibre matrix organization was made to a wild-type phenotype. It remains unclear why no changes were observed in collagen fibre organization in the MUT-treated mice compared to their untreated counterparts.

One explanation may be the importance of fibronectin as a site for integrins in response to mechanical forces. Integrins are found on the surface of cells and act as a link between the extracellular ligands, transmitting forces into the intracellular actin cytoskeleton and communicating signals from the intracellular domains into the ECM. Integrins have a two-way mechano-transduction pathway [18]. The inhibiting of integrins leads to changes in the strain sensing through the ECM [55]. With the decreased amount of fibronectin in the Crouzon mouse suture, there would also be a lack of signalling associated with integrin activation. This may explain the lack of ECM remodelling in the MUT mouse after treatment.

Angiogenesis is an important part of bone remodelling, and mechanical loading has been shown to have a direct impact [18]. None of the groups showed significant differences in the proportion of blood vessels area to the coronal suture area. Although nothing definitive can be said about this observation, there is a developmental coupling between blood vessels and ECM organization. The disorganization seen in the MUT coronal suture ECM may dictate the directionality and development of the blood vessels.

The main limitation of this study was the variation in the mouse model. The early fusion of the coronal suture typically begins at embryonic stages (E18.5), and full closure is commonly achieved by P20 [23,24]. Due to the nature of the loading treatment, it is impossible to identify if a MUT animal has a fully fused suture before the treatment. Not knowing the level of patency of the suture prior to the treatment makes it unclear if the observed results are due to the cyclic loading or the mouse phenotype.

In conclusion, the observed increase in cellular proliferation in the coronal suture after treatment corroborates that there is a cellular response to cyclic mechanical bone loading. Although the hypothesis that cyclic bone loading activates mechanotransduction cannot be validated as the determining pathway at present. Future work will focus on determining the gene expression in the coronal suture using RNA sequencing to understand which pathways are stimulated by cyclic bone loading. Additionally, to further understand the increased proliferation in the treated animals and how it is induced by cyclic bone loading, a time course analysis with EdU will be performed. Furthermore, loading did not significantly affect skull shape and did not change the patency across the coronal suture between treated and untreated MUT animals. To address this, alterations to the treatment protocol will be undertaken to optimize suture patency (i.e. changing the frequency of cyclic loading, changing the number of sessions within a given time frame).

Ethics. All animal experiments were approved by the UK Home Office and performed as part of a Project Licence (number: PP8161503) under the UK Animals (Scientific Procedures) Act 1986. Animal procedures complied with the ARRIVE guidelines and were performed under the supervision of UCL Biological Services.

Data accessibility. Supplementary material is available online [56].

Declaration of AI use. We have not used AI-assisted technologies in creating this article.

Authors' contributions. M.S.: data curation, formal analysis, investigation, methodology, validation, visualization, writing—original draft; M.D.: data curation, formal analysis, investigation, methodology, validation, visualization, writing—original draft; T.Q.: resources, writing—review and editing; D.S.C.: resources, software, writing—review and editing; C.L.: resources, validation, writing—review and editing; A.A.: methodology, resources, software, writing—review and editing; D.M.: methodology, writing—review and editing; O.G.: methodology, resources, writing—review and editing; M.M.: conceptualization, funding acquisition, supervision, writing—review and editing; E.P.: conceptualization, funding acquisition, supervision, writing—review and editing.

All authors gave final approval for publication and agreed to be held accountable for the work performed therein.

Conflict of interest declaration. We declare we have no competing interests.

Funding. This work was supported by the Engineering and Physical Science Research Council (EP/W008092/1; EP/R513143/1—2592407 and EP/T517793/1—2592407) and the NIHR Great Ormond Street Hospital Biomedical Research Centre.

Acknowledgements. All authors contributed to the study's conception and design. Specimen preparation was performed by Miranda Steacy, Marius Didziokas, Tengyang Qiu, Damith Katudampe Vithanage and Erwin Pauws. The custom loading setup was developed by Ali Alazmani. CT data collection and analysis were performed by Marius Didziokas. All histology was performed by Miranda Steacy with the guidance of Oliver Gardner. All image processing was done by Miranda Steacy with the guidance of Dale Moulding. All statistical analysis was done by Miranda Steacy and Marius Didziokas with the guidance of Ce Liang. The first draft of the manuscript was written by Miranda Steacy and Marius Didziokas. All authors commented on previous versions of the manuscript. All authors read and approved the final manuscript. Mehran

Moazen and Erwin Pauws supervised the project and secured the funding. Many thanks to David Longs group for their guidance and support with the endomucin assay and Gabriel Galea for his immunohistochemistry support. Special thanks to Dawn Savery and Benjamin Jevans.





# References


1. Boulet SL, Rasmussen SA, Honein MA. 2008 A population-based study of craniosynostosis in metropolitan Atlanta, 1989–2003. *Am. J. Med. Genet. A* **146A**, 984–991. (doi:10.1002/ajmg.a.32208)
2. Cornelissen M *et al*. 2016 Increase of prevalence of craniosynostosis. *J. Maxillofac. Surg.* **44**, 1273–1279. (doi:10.1016/j.jcms.2016.07.007)
3. Lajeunie E, Le Merrer M, Bonaïti-Pellie C, Marchac D, Renier D. 1995 Genetic study of nonsyndromic coronal craniosynostosis. *Am. J. Med. Genet.* **55**, 500–504. (doi:10.1002/ajmg.1320550422)
4. Johnson D, Wilkie AOM. 2011 Craniosynostosis. *Eur. J. Hum. Genet.* **19**, 369–376. (doi:10.1038/ejhg.2010.235)
5. Richtsmeier JT, Flaherty K. 2013 Hand in glove: brain and skull in development and dysmorphogenesis. *Acta Neuropathol.* **125**, 469–489. (doi:10.1007/s00401-013-1104-y)
6. O'Hara J *et al*. 2019 Syndromic craniosynostosis: complexities of clinical care. *Mol. Syndromol.* **10**, 83–97. (doi:10.1159/000495739)
7. Mathijssen IMJ. 2015 Guideline for care of patients with the diagnoses of craniosynostosis: working group on craniosynostosis. *J. Craniofacial Surg.* **26**, 1735–1807. (doi:10.1097/SCS.0000000000002016)
8. Mehta VA, Bettegowda C, Jallo GI, Ahn ES. 2010 The evolution of surgical management for craniosynostosis. *Neurosurg. Focus* **29**, 1–7. (doi:10.3171/2010.9.FOCUS10204)
9. Herring SW, Rafferty KL, Shin DU, Smith K, Baldwin MC. 2024 Cyclic loading failed to promote growth in a pig model of midfacial hypoplasia. *J. Anat.* **245**, 879–893. (doi:10.1111/joa.14043)
10. Menon S *et al*. 2021 Skeletal stem and progenitor cells maintain cranial suture patency and prevent craniosynostosis. *Nat. Commun.* **12**, 14. (doi:10.1038/s41467-021-24801-6)
11. Moazen M, Hejazi M, Savery D, Jones D, Marghoub A, Alazmani A, Pauws E. 2022 Mechanical loading of cranial joints minimizes the craniofacial phenotype in Crouzon syndrome. *Sci. Rep.* **12**, 9693. (doi:10.1038/s41598-022-13807-9)
12. Yu M *et al*. 2021 Cranial suture regeneration mitigates skull and neurocognitive defects in craniosynostosis. *Cell* **184**, 243–256.(doi:10.1016/j.cell.2020.11.037)
13. Herring SW. 2007 Mechanical influences on suture development and patency. *Front. Oral Health* **12**, 41–56. (doi:10.1159/0000115031)
14. Peptan AI, Lopez A, Kopher RA, Mao JJ. 2008 Responses of intramembranous bone and sutures upon in vivo cyclic tensile and compressive loading. *Bone* **42**, 432–438. (doi:10.1016/j.bone.2007.05.014)
15. Soh SH, Rafferty K, Herring S. 2018 Cyclic loading effects on craniofacial strain and sutural growth in pigs. *Am. J. Orthod. Dentofac. Orthop.* **154**, 270–282. (doi:10.1016/j.ajodo.2017.11.036)
16. Vij K, Mao JJ. 2006 Geometry and cell density of rat craniofacial sutures during early postnatal development and upon in vivo cyclic loading. *Bone* **38**, 722–730. (doi:10.1016/j.bone.2005.10.028)
17. Jaalouk DE, Lammerding J. 2009 Mechanotransduction gone awry. *Nat. Rev. Mol. Cell Biol.* **10**, 63–73. (doi:10.1038/nrm2597)
18. Stewart S, Darwood A, Masouros S, Higgins C, Ramasamy A. 2020 Mechanotransduction in osteogenesis. *Bone Joint Res.* **9**, 1–14. (doi:10.1302/2046-3758.91)
19. Thi MM, Suadicani SO, Schaffler MB, Weinbaum S, Spray DC. 2013 Mechanosensory responses of osteocytes to physiological forces occur along processes and not cell body and require αVβ3 integrin. *Proc. Natl Acad. Sci. USA* **110**, 21012–21017. (doi:10.1073/pnas.1321210110)
20. Humphrey JD, Dufresne ER, Schwartz MA. 2014 Mechanotransduction and extracellular matrix homeostasis. *Nat. Rev. Mol. Cell Biol.* **15**, 802–812. (doi:10.1038/nrm3896)
21. Duncan RL, Turner CH. 1995 Mechanotransduction and the functional response of bone to mechanical strain. *Calcif. Tissue Int.* **57**, 344–358. (doi:10.1007/BF00302070)
22. Wang X, Mao JJ. 2002 Chondrocyte proliferation of the cranial base cartilage upon *in vivo* mechanical stresses. *J. Dent. Res.* **81**, 701–705. (doi:10.1177/154405910208101009)
23. Eswarakumar VP, Horowitz MC, Locklin R, Morriss-Kay GM, Lonai P. 2004 A gain-of-function mutation of Fgfr2c demonstrates the roles of this receptor variant in osteogenesis. *Proc. Natl Acad. Sci. USA* **101**, 12555–12560. (doi:10.1073/pnas.0405031101)
24. Pfaff MJ, Xue K, Li L, Horowitz MC, Steinbacher DM, Eswarakumar VP. 2016 FGFR2c-mediated ERK-MAPK activity regulates coronal suture development. *Dev. Biol.* **415**, 242–250. (doi:10.1073/pnas.0405031101)
25. Ornitz DM, Marie PJ. 2019 Fibroblast growth factors in skeletal development. *Curr. Top. Dev. Biol.* **133**, 195–234. (doi:10.1016/bs.ctdb.2018.11.020)
26. Fragale A, Tartaglia M, Bernardini S, Di Stasi AMM, Di Rocco C, Velardi F, Teti A, Battaglia PA, Migliaccio S. 1999 Decreased proliferation and altered differentiation in osteoblasts from genetically and clinically distinct craniosynostotic disorders. *Am. J. Pathol.* **154**, 1465–1477. (doi:10.1016/s0002-9440(10)65401-6)
27. Oldridge M *et al*. 1995 Mutations in the third immunoglobulin domain of the fibroblast growth factor receptor-2 gene in Crouzon syndrome. *Hum. Mol. Genet.* **4**, 1077–1082. (doi:10.1093/hmg/4.6.1077)
28. Hoshino Y *et al*. 2023 Synchondrosis fusion contributes to the progression of postnatal craniofacial dysmorphology in syndromic craniosynostosis. *J. Anat.* **242**, 387–401. (doi:10.1111/joa.13790)
29. Liu J, Nam HK, Wang E, Hatch NE. 2013 Further analysis of the crouzon mouse: effects of the FGFR2C342Y mutation are cranial bone–dependent. *Calcif. Tissue Int.* **92**, 451–466. (doi:10.1007/s00223-013-9701-2)
30. Martínez-Abadías N, Motch SM, Pankratz TL, Wang Y, Aldridge K, Jabs EW, Richtsmeier JT. 2013 Tissue-specific responses to aberrant FGF signaling in complex head phenotypes. *Dev. Dyn.* **242**, 80–94. (doi:10.1002/dvdy.23903)
31. Perlyn CA, DeLeon VB, Babbs C, Govier D, Burell L, Darvann T, Kreiborg S, Morriss-Kay G. 2006 The craniofacial phenotype of the Crouzon mouse: analysis of a model for syndromic craniosynostosis using three-dimensional MicroCT. *Cleft Palate Craniofac. J.* **43**, 740–748. (doi:10.1597/05-212)
32. Peskett E, Kumar S, Baird W, Jaiswal J, Li M, Patel P, Britto JA, Pauws E. 2017 Analysis of the Fgfr2C342Y mouse model shows condensation defects due to misregulation of Sox9 expression in prechondrocytic mesenchyme. *Biol. Open* **6**, 223–231. (doi:10.1242/bio.022178)
33. Richtsmeier JT, Baxter LL, Reeves RH. 2000 Parallels of craniofacial maldevelopment in down syndrome and Ts65Dn mice. *Dev. Dyn.* **217**, 137–145. (doi:10.1002/(sici)1097-0177(200002)217:23.0.co;2-n)
34. Motch Perrine SM, Cole TM, Martínez-Abadías N, Aldridge K, Jabs EW, Richtsmeier JT. 2014 Craniofacial divergence by distinct prenatal growth patterns in Fgfr2 mutant mice. *BMC Dev. Biol.* **14**, 8. (doi:10.1186/1471-213X-14-8)

35. Schmidt U, Weigert M, Broaddus C, Myers G. 2018 Cell detection with star-convex polygons (eds AF Frangi, JA Schnabel, C Davatzikos, C Alberola-López, G Fichtinger). In *Medical Image Computing and Computer Assisted Intervention—MICCAI 2018: 21st International Conference, Granada, Spain, September 16–20, 2018, proceedings, part II*, pp. 265–273. Heidelberg, Germany: Springer International Publishing. (doi:10.1007/978-3-030-00934-2_30)
36. Fonck E, Feigl GG, Fasel J, Sage D, Unser M, Rüfenacht DA, Stergiopulos N. 2009 Effect of aging on elastin functionality in human cerebral arteries. *Stroke* **40**, 2552–2556. (doi:10.1161/strokeaha.108.528091)
37. Jäger I, Fratzl P. 2000 Mineralized collagen fibrils: a mechanical model with a staggered arrangement of mineral particles. *Biophys.* **79**, 1737–1746. (doi:10.1016/S0006-3495(00)76426-5)
38. Lanfer B, Freudenberg U, Zimmermann R, Stamov D, Körber V, Werner C. 2008 Aligned fibrillar collagen matrices obtained by shear flow deposition. *Biomaterials* **29**, 3888–3895. (doi:10.1016/j.biomaterials.2008.06.016)
39. Ma C, Wang H, Chi Y, Wang Y, Jiang L, Xu N, Wu Q, Feng Q, Sun X. 2021 Preparation of oriented collagen fiber scaffolds and its application in bone tissue engineering. *Appl. Mater. Today* **22**, 100902. (doi:10.1016/j.apmt.2020.100902)
40. Didziokas M, Jones D, Alazmani A, Steacy M, Pauws E, Moazen M. 2024 Multiscale mechanical characterisation of the craniofacial system under external forces. *Biomech. Model. Mechanobiol.* **23**, 675–685. (doi:10.1007/s10237-023-01799-y)
41. Liang C *et al*. 2024 A physico-mechanical model of postnatal craniofacial growth in human. *iScience* **27**, 110617. (doi:10.1016/j.isci.2024.110617)
42. Marghoub A, Libby J, Babbs C, Pauws E, Fagan MJ, Moazen M. 2018 Predicting calvarial growth in normal and craniosynostotic mice using a computational approach. *J. Anat.* **232**, 440–448. (doi:10.1111/joa.12764)
43. Didziokas M, Steacy M, Qiu T, Marghoub A, Alazmani A, Pauws E, Moazen M. 2025 Regional variability in craniofacial stiffness: a study in normal and Crouzon mice during postnatal development. *Biomech. Model. Mechanobiol.* **24**, 1207–1222. (doi:10.1007/s10237-025-01962-7)
44. Parsons TE, Weinberg SM, Khaksarfard K, Howie RN, Elsalanty M, Yu JC, Cray JJ. 2014 Craniofacial shape variation in Twist1+/- mutant mice. *Anat. Rec.* **297**, 826–833. (doi:10.1002/ar.22899)
45. Zimmermann B, Moegelin A, de Souza P, Bier J. 1998 Morphology of the development of the sagittal suture of mice. *Anat. Embryol.* **197**, 155–165. (doi:10.1007/s004290050127)
46. Iseki S, Wilkie AOM, Morriss-Kay GM. 1999 Fgfr1 and Fgfr2 have distinct differentiation- and proliferation-related roles in the developing mouse skull vault. *Development* **126**, 5611–5620. (doi:10.1242/dev.126.24.5611)
47. Chen JC, Hoey DA, Chua M, Bellon R, Jacobs CR. 2016 Mechanical signals promote osteogenic fate through a primary cilia-mediated mechanism. *FASEB J.* **30**, 1504–1511. (doi:10.1096/fj.15-276402)
48. Hoey DA, Tormey S, Ramcharan S, O'Brien FJ, Jacobs CR. 2012 Primary cilia-mediated mechanotransduction in human mesenchymal stem cells. *Stem Cells* **30**, 2561–2570. (doi:10.1002/stem.1235)
49. Gronowicz GA, Fall PM, Raisz LG. 1994 Prostaglandin E2 stimulates preosteoblast replication: an autoradiographic study in cultured fetal rat calvariae. *Exp. Cell Res.* **212**, 314–320. (doi:10.1006/excr.1994.1149)
50. Baroni T, Lilli C, Marinucci L, Bellocchio S, Pezzetti F, Carinci F, Stabellini G, Balducci C, Locci P. 2002 Crouzon's syndrome: differential in vitro secretion of bFGF, TGFbeta I isoforms and extracellular matrix macromolecules in patients with FGFR2 gene mutation. *Cytokine* **19**, 94–101. (doi:10.1006/cyto.2002.0877)
51. White HE, Goswami A, Tucker AS. 2021 The intertwined evolution and development of sutures and cranial morphology. *Front. Cell Dev. Biol.* **9**, 653579. (doi:10.3389/fcell.2021.653579)
52. Warren SM, Walder B, Dec W, Longaker MT, Ting K. 2008 Confocal laser scanning microscopic analysis of collagen scaffolding patterns in cranial sutures. *J. Craniofac. Surg.* **19**, 198–203. (doi:10.1097/scs.0b013e31815c8a9a)
53. Huang CC. 1987 Bone resorption in experimental otosclerosis in rats. *Am. J. Otolaryngol.* **8**, 332–341. (doi:10.1016/s0196-0709(87)80052-2)
54. Yu L, Hou Y, Xie W, Cuellar-Camacho JL, Wei Q, Haag R. 2020 Self-strengthening adhesive force promotes cell mechanotransduction. *Adv. Mater.* **32**, e2006986. (doi:10.1002/adma.202006986)
55. Streuli C. 1999 Extracellular matrix remodelling and cellular differentiation. *Curr. Opin. Cell Biol.* **11**, 634–640. (doi:10.1016/s0955-0674(99)00026-5)
56. Steacy M *et al*. 2026 . Supplementary material from: Mechanical bone loading effects on morphology and mechanobiology in the coronal suture of Crouzon mice. Figshare. (doi:10.6084/m9.figshare.c.8382150)